Relativistic Many-Body Calculations of Magnetic Dipole Transitions in Be-Like Ions

Physica Scripta. Vol. 60, 46–53, 1999

Relativistic Many-Body Calculations of Magnetic Dipole Transitions in Be-Like Ions

U. I. Safronova, W. R. Johnson and A. Derevianko

Department of Physics, University of Notre Dame, Notre Dame, IN 46556, USA

Received November 12, 1998; accepted November 17, 1998

PACS Ref: 32.70.Cs, 31.15.Md, 31.25.-v, 31.30.Jv

Abstract

Reduced matrix elements and transition rates are calculated for all magnetic dipole (M1) transitions within $2l2l'$ configurations and for some $2l3l'$ - $2l2l'$ transitions in Be-like ions with nuclear charges ranging from $Z = 4$ to 100. Many-body perturbation theory (MBPT), including the Breit interaction, is used to evaluate retarded M1 matrix elements. The calculations start with a $(1s)^2$ Dirac-Fock potential and include all possible $n = 2$ configurations, leading to 4 odd-parity and 6 even-parity states, and some $n = 3$ configurations. First-order perturbation theory is used to obtain intermediate coupling coefficients. Second-order MBPT is used to determine the matrix elements, which are evaluated for all 11 M1 transitions within $2l2l'$ configurations and for 35 M1 transitions between $2l3l'$ and $2l2l'$ states. The transition energies used in the calculation of oscillator strengths and transition rates are obtained from second-order MBPT. The importance of negative-energy contributions to M1 transition amplitudes is discussed.

1. Introduction

Studies of M1 transitions are much less complete than studies of E1 transitions, as testified to by the small number of theoretical papers that have been devoted to M1 transitions [1–7] during the past thirty years. This lack of interest is associated in part with the fact that the probability of M1 transitions is several orders magnitude smaller than the probability of E1 transitions. In spite of the small probability, $1s^2\ {}^1S_0$ – $1s2s\ {}^3S_1$ M1 transitions have been observed in the solar corona and M1 transitions between states within $1s^22s^22p^3$ configurations in OII have been observed in spectra of gaseous nebulae. Recently [8], the lifetime of the $1s^22s2p\ {}^3P_2$ level of Ar XV was measured using metastable Ar^{14+} ions produced by an electron cyclotron resonance ion source. It was found [8] that the rate derived from the measured lifetime differed significantly from both nonrelativistic [9] and relativistic [7] calculations of M1 transition rates. It should be noted that, for M1 transitions within a single configuration, differences between relativistic and nonrelativistic calculations are insignificant.

The purpose of this paper to calculate the forbidden $2s^2$–2s3s, 2s2p–2p3s, and 2s2p–2s3p M1 transitions in berylliumlike ions. We also calculate M1 transitions within 2s2p and $2p^2$ configurations, and confirm that our results for allowed $2l$–$2l$ transitions are in good agreement with other theoretical results.

In the present paper, we use relativistic many-body perturbation theory (MBPT) to determine reduced matrix elements and transition rates for all lines in $2l2l'$ configurations and for some $2l3l' - 2l2l'$ lines in Be-like ions with nuclear charges ranging from $Z = 4$ to 100. Our calculations start from a $(1s)^2$ Dirac-Fock potential, and include all possible $n = 2$ configurations, leading to 4 odd-parity and 6 even-parity states; they also include some $n = 3$ configurations. Second-order MBPT is used to determine the matrix elements, which are evaluated for the 11 transitions inside $2l2l'$ configurations and for 35 transitions between states of $2l3l'$ and $2l2l'$ configurations. The transition energies used in the calculation of transition rates are evaluated using second-order MBPT. Negative-energy contributions to the transition amplitudes are included. The present calculations provide a theoretical benchmark for future experiments and calculations.

2. Method

In this section, we write down and discuss the relativistic MBPT formulas for first- and second-order transition matrix elements in atomic systems with two valence electrons. It should be noted that the primary difference in the theoretical expressions for E1 and M1 transition matrix elements occurs in the first-order. Details of second-order MBPT calculations for E1 matrix elements were presented in [10]; here we give the expression for the first-order M1 matrix element only and refer the reader to Ref. [10] for a discussion of second-order diagrams. The present results are given in the Coulomb gauge. It should be noted that gauge transformations of the type considered in [10] have no effect on M1 matrix elements.

2.1. *Basic formulas*

The first-order reduced dipole matrix element $M^{(1)}$ for the transition between two states $vw(J) - v'w'(J')$ is [11]

$$M^{(1)}[v_1w_1(J)-v_2w_2(J')] = \sqrt{[J][J']}\sum_{vw}\sum_{v'w'}\mathcal{S}^J(v_1w_1, vw)\mathcal{S}^{J'}(v_2w_2, v'w') \times (-1)^{1+j_w+j_{v'}}\begin{Bmatrix} J & J' & 1 \\ j_{v'} & j_w & j_v \end{Bmatrix} M_{v'w}\delta_{vw'}, \qquad (1)$$

where $[J] = 2J + 1$. The quantity $\mathcal{S}^J(v_1w_1, vw)$ is a symmetry coefficient defined by

$$\mathcal{S}^J(v_1w_1, vw) = \eta_{v_1w_1}\left[\delta_{v_1v}\delta_{w_1w} + (-1)^{j_v+j_w+J+1}\delta_{v_1w}\delta_{w_1v}\right], \qquad (2)$$

where η_{vw} is a normalization factor given by

$$\eta_{vw} = \begin{cases} 1 & \text{for } w \neq v \\ 1/\sqrt{2} & \text{for } w = v. \end{cases}$$

The magnetic dipole matrix element M_{vw}, which includes

retardation, is given by

$$M_{vw} = \langle -\kappa_v \| C_1 \| \kappa_w \rangle \frac{6}{\alpha k} \int_0^\infty \mathrm{d}r \frac{(\kappa_v + \kappa_w)}{2} j_1(kr) \times [G_v(r)F_w(r) + F_v(r)G_w(r)]\,. \tag{3}$$

Here κ_v is the angular momentum quantum number [$\kappa_v = \mp(j_v + \frac{1}{2})$ for $j_v = (l_v \pm \frac{1}{2})$], and $k = \omega\alpha$, where $\omega = \varepsilon_w - \varepsilon_v$ is the photon energy and α is the fine-structure constant. The quantity $C_{1q}(\hat{r})$ is a normalized spherical harmonic. The functions $G_a(r)$ and $F_a(r)$ are large- and small-component radial Dirac wave functions, respectively.

The nonrelativistic limit is different for transitions inside of one configurations, $n_v = n_w$, and transitions between different configurations, $n_v \neq n_w$. For the case $n_v = n_w$, we obtain

$$M_{vw}^{\mathrm{NR}} = -\langle -\kappa_v \| C_1 \| \kappa_w \rangle (\kappa_v + \kappa_w - 1) \frac{(\kappa_v + \kappa_w)}{2} \times \int_0^\infty \mathrm{d}r P_v(r) P_w(r)\,, \tag{4}$$

where $P_v(r)$ is a nonrelativistic limit the large-component radial wave function $G_v(r)$. The case $n_v \neq n_w$ was considered in [11–16] for $1s^2\ {}^1S_0$–$1s2s\ {}^3S_1$ transitions. The nonrelativistic limit in this case is proportional to Z^2, and for transitions with $l_v = l_w = 0$ the matrix element is given by

$$M_{vw}^{\mathrm{NR}} = -(\alpha Z)^2 \sqrt{\frac{2}{3}} \times \left[\frac{3}{Z} \int_0^\infty \frac{1}{r} \mathrm{d}r P_v(r) P_w(r) + \frac{\omega^2}{2Z^2} \int_0^\infty r^2 \mathrm{d}r P_v(r) P_w(r) \right]. \tag{5}$$

Using hydrogenic wave functions, we find

$$M_{1s2s}^{\mathrm{NR}} = -(\alpha Z)^2 \frac{16}{27\sqrt{3}}, \qquad M_{2s3s}^{\mathrm{NR}} = -(\alpha Z)^2 \frac{2^4 23}{5^5}. \tag{6}$$

Second-order contributions to E1 reduced matrix elements are written out in [10]. It is only necessary to replace the quantities Z_{vw} in Ref. [10] by M_{vw} to obtain the corresponding second-order contributions to M1 reduced matrix elements. The reduced matrix element for the derivative term is given by

$$M^{(\mathrm{derv})}[vw(J) - v'w'(J')] = \alpha\, (E_{vw}^{(1)} - E_{v'w'}^{(1)}) \times P^{(\mathrm{derv})}[vw(J) - v'w'(J')], \tag{7}$$

where $E_{vw}^{(1)}$, is the first-order correction to the energy given by Eqs. (2.8–2.10) of Ref. [21]. The quantity $P^{(\mathrm{derv})}$ introduced

Table I. *Uncoupled* M1 *reduced matrix for* Fe^{+22} *Notation:* $np = np_{3/2}$, $np^* = np_{1/2}$, $3d = 3d_{5/2}$, $3d^* = 3d_{3/2}$

(a) Coulomb Interaction: $vw[J]$	$v'w'[J']$	$M^{(1)}$	$P^{(\mathrm{derv})}$	$M^{(\mathrm{RPA})}$	$M^{(\mathrm{corr})}$
2s2p*[0]	2s2p*[1]	1.154620	1.154620	–0.000023	0.000027
2s2p*[0]	2s2p [1]	0.814777	0.814777	0.000065	–0.000016
2s2p [1]	2s2p [1]	2.848083	2.848083	0.000112	0.000137
2p*2p [2]	2p*2p [2]	6.365538	6.365538	0.000006	0.000800
2p*2p [2]	2p2p [2]	–1.288276	–1.288275	–0.000103	–0.000059
2p2p [2]	2p*2p [2]	–1.288276	–1.288275	–0.000103	–0.000059
2p2p [2]	2p2p [2]	7.279830	7.279830	0.000110	0.000598
2s2s [0]	2s3s [1]	0.003755	0.000018	0.000053	–0.000243
2s2s [0]	2s3d*[1]	–0.001221	0.000694	0.000002	0.000131
2p2p [0]	2p3p [1]	0.005110	0.001239	–0.000024	–0.000325
2s2p*[1]	2s3p*[0]	–0.001347	–0.001787	–0.000023	–0.000102
2s2p [1]	2p3d*[0]	–0.000611	0.000347	0.000001	–0.000051
(b) Breit Interaction with factor 10^3 vw[J]	v′w′[J′]	$B^{(\mathrm{HF})}$	$B^{(\mathrm{RPA})}$	$B^{(\mathrm{corr})}$	$B^{(2)}$
2s2p*[0]	2s2p*[1]	–0.214620	0.153805	–0.024369	–0.085184
2s2p*[0]	2s2p [1]	–0.069154	0.015593	–0.039520	–0.093081
2s2p [1]	2s2p [1]	0.012768	0.102957	–0.095533	0.020192
2p*2p [2]	2p*2p [2]	0.395632	–0.210116	–0.398355	–0.212839
2p*2p [2]	2p2p [2]	0.109343	–0.024654	–0.064385	0.020303
2p2p [2]	2p*2p [2]	0.109343	–0.024654	–0.064385	0.020303
2p2p [2]	2p2p [2]	0.042419	0.131645	–0.155396	0.018668
2s2s [0]	2s3s [1]	–0.012301	0.031090	0.039747	0.058535
2s2s [0]	2s3d*[1]	0.004822	–0.014542	–0.069244	–0.078964
2p2p [0]	2p3p [1]	–0.012286	–0.031559	0.093758	0.049912
2s2p*[1]	2s3p*[0]	0.111038	–0.090110	–0.101976	–0.081049
2s2p [1]	2p3d*[0]	0.002411	–0.007271	0.013019	0.008159

above is given by

$$P^{(\mathrm{derv})}[v_1w_1(J) - v_2w_2(J')] = \sqrt{[J][J']}\sum_{vw}\sum_{v'w'} S^J(v_1w_1, vw)S^{J'}(v_2w_2, v'w') \times (-1)^{1+j_w+j_{v'}} \begin{Bmatrix} J & J' & 1 \\ j_{v'} & j_w & j_v \end{Bmatrix} M^{(\mathrm{derv})}_{v'w}\delta_{vw'}, \quad (8)$$

where

$$M^{(\mathrm{derv})}_{vw} = \langle\kappa_v\|C_1\|\kappa_w\rangle \frac{6}{\alpha k}\int_0^\infty \mathrm{d}r \frac{(\kappa_v+\kappa_w)}{2}[j_1(kr) - (kr)j_2(kr)] \times [G_v(r)F_w(r) + F_v(r)G_w(r)]\,. \quad (9)$$

All second-order correlation corrections above are from the residual Coulomb interaction. To include correlation corrections from the Breit interaction, the Coulomb matrix element $X_k(abcd)$ must be modified according to the rule:

$$X_k(abcd) \to X_k(abcd) + M_k(abcd) + N_k(abcd). \quad (10)$$

The magnetic radial integrals M_k and N_k are defined by Eqs.(A4, A5) in Ref. [17].

2.2. *Uncoupled matrix elements*

In Table I, we list values of $M^{(1)}$, $M^{(\mathrm{HF})}$, $M^{(\mathrm{RPA})}$, $M^{(\mathrm{corr})}$, and $P^{(\mathrm{derv})}$ for transitions in Be-like iron, $Z = 26$. Two types of transitions are presented: those with no change of principal quantum number (2–2 transitions) and those with a unit change of principal quantum number (2–3 transitions). It should be noted that the contribution from the HF diagram, $M^{(\mathrm{HF})}$, vanishes in the present calculation since we use HF basis functions. In the table, we use the label B to denote the Breit contributions and we tabulate $1000\times B^{(\mathrm{HF})}$, $1000\times B^{(\mathrm{RPA})}$, $1000\times B^{(\mathrm{corr})}$, together with the sum, $1000\times B^{(2)}$. It can be seen from Table I that the largest difference (a factor of 1000) between two types of transitions occurs in the values of the first-order matrix element $M^{(1)}$. However, there are no large differences for the second-order diagram contributions ($M^{(\mathrm{RPA})}$, $M^{(\mathrm{corr})}$) and Breit contributions ($B^{(\mathrm{HF})}$, $B^{(\mathrm{RPA})}$, $B^{(\mathrm{corr})}$). To interpret this observation we consider the Z-dependence of a typical second-order diagram

$$M^{(\mathrm{corr})} \sim \sum_{iw\notin P'} \frac{M_{iv}g_{v'w'wi}}{\varepsilon_i + \varepsilon_w - \varepsilon_{v'} - \varepsilon_{w'}}\,. \quad (11)$$

Here P' denotes the model space of $w'v'$. The intermediate state energy ε_i takes both positive, $\varepsilon_i > mc^2$, and negative, $\varepsilon_i < -mc^2$, values. To begin, we focus on the positive-energy contribution to such diagrams. The magnetic-dipole matrix element M_{iv} involving an intermediate state can be either of order of 1, provided $|i\rangle = |v\rangle$ is allowed by the condition $vw \notin P'$, or of order of $(\alpha Z)^2$, otherwise. The leading term of Coulomb matrix element $X_k(abcd)$ is proportional to Z. The Breit interaction is proportional to α^2Z^3 and ε_i is proportional to Z^2. As a result, we obtain two different Z-dependences for $M^{(\mathrm{corr})}$ and $B^{(\mathrm{corr})}$:

$$M^{(\mathrm{corr})} \propto \begin{cases} 1/Z & \text{for } n_i = n_v \\ \alpha^2 Z & \text{for } n_i \neq n_v \end{cases}, \quad B^{(\mathrm{corr})} \propto \begin{cases} \alpha^2 Z & \text{for } n_i = n_v \\ \alpha^4 Z^3 & \text{for } n_i \neq n_v. \end{cases}$$

For transitions inside the same model space ($2l_12l_2 - 2l_32l_4$), the upper case is never realized, since the condition $vw \notin P'$ is not satisfied. The upper case is realized for transitions such as $2s2p_{3/2} - 2s3p_{3/2}$. For such transitions, the lowest-order matrix element is suppressed by $(\alpha Z)^2$; thus, the leading contribution to uncoupled matrix elements arises from the second-order diagrams.

2.3. *Contribution from the negative-energy states*

Ab initio relativistic calculations require a careful treatment of negative-energy states (virtual electron-positron pairs), which, if included improperly, lead to the *continuum dissolution* problem discussed by Sucher [18]. A common approach to relativistic calculations is to use the *no-pair* Hamiltonian, which excludes the negative-energy states (NES) [18,19]. However, the NES contribution appears in the evaluation of transition amplitudes. In the second-order expressions (11), such contribution explicitly arises from the terms in the sum over states i and n for which $\varepsilon_i < -mc^2$. The effect of the NES contributions to M1-amplitudes has been studied recently for heliumlike ions in [15,16,20]. In Ref. [20] it was demonstrated that for nonrelativistically forbidden magnetic-dipole transitions the relative contribution of NES grows for low Z as $1/Z$ in calculations using a model-potential basis.

To understand the relative importance of NES for Be-like ions, we consider the scaling of leading terms in an αZ expansion of various diagrams for uncoupled matrix elements. As discussed in Section B, the leading regular *no-pair* contribution to the total value of uncoupled matrix element for $2l_12l_2 - 2l_33l_4$ transitions scales either as $(\alpha Z)^2$ or as $1/Z$, depending on the selection rules intermediate states. The leading term for $2l_12l_2 - 2l_32l_4$ transitions is of order of 1 and arises from the non-relativistically allowed lowest order. The analysis of the NES contribution is similar to that given in Ref. [20]. First, we notice that the energy denominator can be replaced by $-2mc^2$ with an accuracy of $(\alpha Z)^2$. Further, we take into account that the meaning of "large" and "small" components for a negative-energy state is reversed, i.e., the large component is αZ times smaller than the small component. The magnetic-dipole matrix element M_{iv} couples the large component of the positive-energy state $|v\rangle$ and the small component of the negative-energy state $|i\rangle$. Therefore, as can be seen from Eq. (3), $M_{iv} \propto 1/\alpha Z$. Applying the same argument to the Coulomb and Breit matrix elements, we arrive at the conclusion that the NES contribution scales as $\alpha^2 Z$ for both Breit and Coulomb contributions.

$$M^{(\mathrm{corr})}_- \sim B^{(\mathrm{corr})}_- \sim \alpha^2 Z\,.$$

We see that the relative contribution of NES to uncoupled magnetic-dipole amplitude scales as $\alpha^2 Z$ for $2l_12l_2 - 2l_32l_4$ transitions, and as $(\alpha Z)^2$ or $1/Z$ for $2l_12l_2 - 2l_33l_4$ transitions, depending on the leading order of the regular *no-pair* contribution.

2.4. *Coupled matrix elements*

Physical two-particle states are linear combinations of uncoupled two-particle states (vw) in the model space that have fixed values of angular momentum and parity; consequently, transition amplitudes between physical states are linear combinations of the uncoupled transition matrix elements given in Table I. Expansion coefficients and energies

are obtained by diagonalizing the effective Hamiltonian as discussed in [21]. The first-order expansion coefficient $C_1^\lambda(vw)$ is the λ-th eigenvector of the first-order effective Hamiltonian, and E_1^λ is the corresponding eigenvalue. In the present calculation, both Coulomb and Breit interactions are included in the first-order effective Hamiltonian. The coupled transition matrix element between the I-th, initial eigenstate which has angular momentum J and the F-th final state which has angular momentum J' is given by

$$\begin{aligned} Q^{(1+2)}(I-F) = \frac{1}{E_1^I - E_1^F} \sum_{vw} \sum_{v'w'} C_1^I(vw) C_1^F(v'w') \\ \times \big\{ [\varepsilon_{vw} - \varepsilon_{v'w'}] \big[M^{(1+2)}[vw(J) - v'w'(J')] \\ + B^{(2)}[vw(J) - v'w'(J')] \big] \\ + \big[E_1^I - E_1^F - \varepsilon_{vw} + \varepsilon_{v'w'} \big] \\ \times P^{(\mathrm{derv})}[vw(J) - v'w'(J')] \big\}. \end{aligned} \tag{12}$$

Here, $\varepsilon_{vw} = \varepsilon_v + \varepsilon_w$ and $M^{(1+2)} = M^{(1)} + M^{(\mathrm{RPA})} + M^{(\mathrm{corr})}$. Using these formulas and the results for uncoupled reduced matrix elements given in Table I, we transform from uncoupled reduced matrix elements to intermediate coupled reduced matrix elements between physical states.

To cite a specific example, in Fig. 1 we present the mixing coefficients as functions of Z for the 2s3p ^{3}P$_1$ level. It should be noted that the odd parity complex with $J = 1$ includes 7 two-particle states 2s3p$_{1/2}$, 2s3p$_{3/2}$, 2p$_{1/2}$3s, 2p$_{3/2}$3s, 2p$_{1/2}$3d$_{3/2}$, 2p$_{3/2}$3d$_{3/2}$, and 2p$_{3/2}$3d$_{5/2}$. After diagonalization, the 7 eigenvectors are labeled 2s3p ^{1}P$_1$, 2s3p ^{3}P$_1$, 2p3s ^{3}P$_1$, 2p3s ^{1}P$_1$, 2p3d ^{3}D$_1$, 2p3d ^{3}P$_1$, and 2p3d ^{1}P$_1$. These states form the complex of final states, labeled by "F" in Eq. (18),

$$\begin{aligned} \Psi(F) = C^F(2\mathrm{s}3\mathrm{p}_{1/2})\Psi(2\mathrm{s}3\mathrm{p}_{1/2}) + C^F(2\mathrm{s}3\mathrm{p}_{3/2})\Psi(2\mathrm{s}3\mathrm{p}_{3/2}) \\ + C^F(2\mathrm{p}_{1/2}3\mathrm{s})\Psi(2\mathrm{p}_{1/2}3\mathrm{s}) + C^F(2\mathrm{p}_{3/2}3\mathrm{s})\Psi(2\mathrm{p}_{3/2}3\mathrm{s}) \\ + C^F(2\mathrm{p}_{1/2}3\mathrm{d}_{3/2})\Psi(2\mathrm{p}_{1/2}3\mathrm{d}_{3/2}) \\ + C^F(2\mathrm{p}_{3/2}3\mathrm{d}_{3/2})\Psi(2\mathrm{p}_{3/2}3\mathrm{d}_{3/2}) \\ + C^F(2\mathrm{p}_{3/2}3\mathrm{d}_{5/2})\Psi(2\mathrm{p}_{3/2}3\mathrm{d}_{5/2}). \end{aligned} \tag{13}$$

In Fig. 1, we show the Z-dependence of the 7 coefficients $C^F(vw)$ in the above expansion. We can see from this figure that the largest contribution to the 2s3p ^{3}P$_1$ level in the range $Z = 6$–12 arises from the 2s3p$_{1/2}$ state, for $Z = 13$–50 is from the 2s3p$_{3/2}$ state, but for $Z = 51$–100 the contribution of the 2p$_{1/2}$3s state becomes dominant. We observe similar complex behavior of mixing coefficients for other levels.

The importance of these mixing coefficients is demonstrated in Fig. 2. We can see a series deep minima in Fig. 2, where the M1 coupled matrix elements are shown as functions of Z with the single initial state 2s2p ^{3}P$_0$ and seven final states from the odd-parity complex with $J = 1$. Most of these minima are at the mixing coefficient crossings shown in Fig. 2. We investigated the Z-dependence of the uncoupled matrix elements $M^{(1+2)} = M^{(1)} + M^{(\mathrm{RPA})} + M^{(\mathrm{corr})}$ and $B^{(2)}$ for the seven uncoupled matrix elements with $(vw) = 2\mathrm{s}2\mathrm{p}_{1/2}[0]$ and $(v'w') = 2\mathrm{s}3\mathrm{p}_{1/2}[1]$, 2s3p$_{3/2}$[1], 2p$_{1/2}$3s[1], 2p$_{3/2}$3s[1], 2p$_{1/2}$3d$_{3/2}$[1], 2p$_{3/2}$3d$_{3/2}$[1], and 2p$_{3/2}$3d$_{5/2}$[1]. There are no peaks for these matrix elements. There are minima in two curves for $B^{(2)}$, but the contributions of these matrix elements are 100 times smaller than the contribution of the other five matrix elements for $B^{(2)}$. Moreover, they do not effect the coupled matrix elements shown in Fig. 2. We conclude that the mixing coefficients alone are responsible for the minima in the coupled matrix elements.

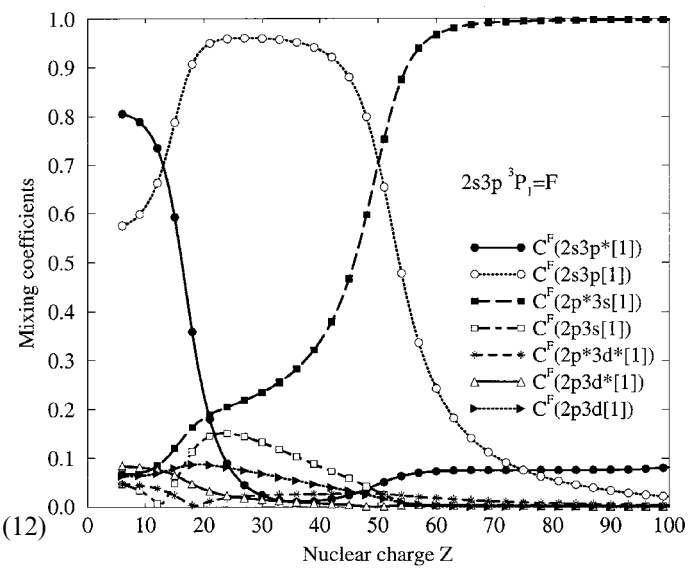

Fig. 1. Z-dependence of the mixing coefficients for 2s3p ^{3}P$_1$ level.

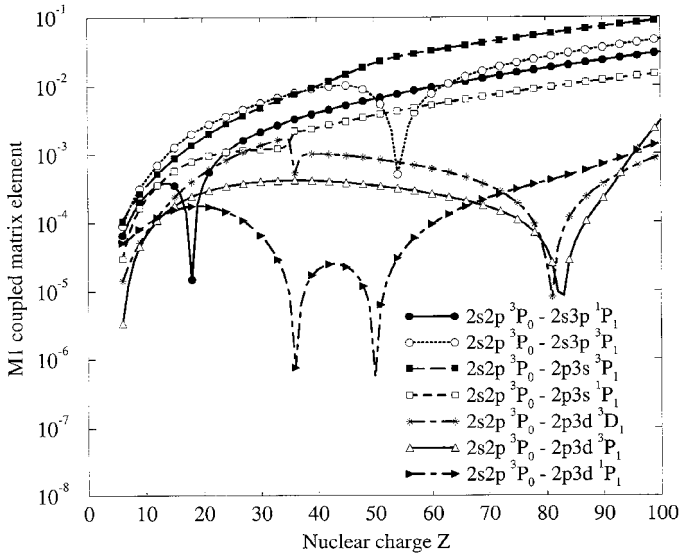

Fig. 2. Z-dependence of the M1 coupled matrix elements.

Let us return to the discussion of negative-energy contributions. In Table II, we list the values of the coupled reduced matrix elements calculated with and without NES contribution for Fe^{+22}. We can see that the relative contribution of NES is ~0.03% for transitions inside the $2l2l'$ configuration space and ~3% for $2l_12l_2 - 2l_33l_4$ transitions. Since the scaling of NES contribution, discussed in Section B, does not depend on a transition, we devise the qualitative rule: the negative-energy contribution is most important for the weakest transitions in a given transition array. Predictions from this rule can be easily verified by analyzing values in Table II.

Figure 3 illustrates the relative size of contributions of NES to several transitions inside the $2l2l'$ configuration space. We observe very small relative NES contributions for these transitions. These contributions grow with increasing nuclear charge, in agreement with the expected Z-dependence, and are bound by 0.3% at $Z = 100$. The relatively small NES effect

Table II. *Coupled reduced matrix elements* M1 *for* Fe^{+22}. *Comparison* M1 *– calculated with (a) and without (b) negative–energy component. Notation:* $np = np_{3/2}$, $np^* = np_{1/2}$, $3d = 3d_{5/2}$, $3d^* = 3d_{3/2}$.

$l_1 l_2$ LSJ	$l_1' l_2'$ $L'S'J'$	M1[a]	M1[b]	$vw[J]$	$v'w'[J']$
2s2p $^3P_0$	2s2p $^3P_1$	1.396484	1.396742	2s2p*[0]	2s2p*[1]
2s2p $^3P_0$	2s2p $^1P_1$	0.215871	0.215909	2s2p*[0]	2s2p[1]
2s2p $^3P_2$	2s2p $^3P_1$	1.559213	1.559367	2s2p[2]	2s2p*[1]
2s2p $^3P_2$	2s2p $^1P_1$	0.242869	0.242893	2s2p[2]	2s2p[1]
2s^2 $^1S_0$	2s3s $^3S_1$	0.003715	0.003701	2s2s[0]	2s3s[1]
2s^2 $^1S_0$	2s3d $^3D_1$	0.001171	0.001161	2s2s[0]	2s3d*[1]
2p^2 $^3P_0$	2s3s $^3S_1$	0.001237	0.001271	2p*2p*[0]	2s3s[1]
2p^2 $^3P_0$	2p3p $^3D_1$	0.006483	0.006535	2p*2p*[0]	2p*3p[1]
2p^2 $^3P_0$	2p3p $^3S_1$	0.001821	0.001835	2p*2p*[0]	2p3p*[1]
2p^2 $^3P_0$	2p3p $^3P_1$	0.002964	0.002915	2p*2p*[0]	2p3p [1]
2p^2 $^1S_0$	2p3p $^1P_1$	0.000964	0.000997	2p2p[0]	2p*3p*[1]
2p^2 $^1S_0$	2p3p $^3D_1$	0.001608	0.001629	2p2p[0]	2p*3p[1]
2p^2 $^1S_0$	2p3p $^3S_1$	0.001354	0.001321	2p2p[0]	2p3p*[1]
2s2p $^3P_1$	2s3p $^3P_0$	0.001906	0.001932	2s2p*[1]	2s3p*[0]
2s2p $^3P_1$	2p3s $^3P_0$	0.002133	0.002062	2s2p*[1]	2p*3s[0]
2s2p $^3P_0$	2s3p $^1P_1$	0.001422	0.001396	2s2p*[0]	2s3p*[1]
2s2p $^3P_0$	2p3s $^3P_1$	0.003406	0.003340	2s2p*[0]	2p*3s[1]
2s2p $^3P_0$	2p3s $^1P_1$	0.001119	0.001143	2s2p*[0]	2p3s[1]

is explained by the non-relativistically allowed character of the transitions inside the $2l2l'$ configuration space, the relative contribution of the second-order diagrams being comparably small. The transitions between $2l_1 2l_2$ and $2l_3 3l_4$ configuration spaces are non-relativistically forbidden; therefore, the NES effect on the transition amplitudes is amplified. To illustrate this assertion, in Fig. 4 we present the Z-dependence of relative NES contribution to the line strength (or rate) for several $2l_1 2l_2 - 2l_3 3l_4$ transitions. We see that the ratio $(S_{n+p} - S_p)/S_{n+p}$ for these transitions can be as large as 25% and the NES contribution is the most important for low-Z calculations, in accordance with the expected Z dependence. On this plot, we can see several irregularities which are the reflections of minima in the total values of M1 coupled matrix elements. It is worth emphasizing that the contribution from the negative-energy states can be comparable to the regular *no-pair* contribution for transitions involving different configuration spaces.

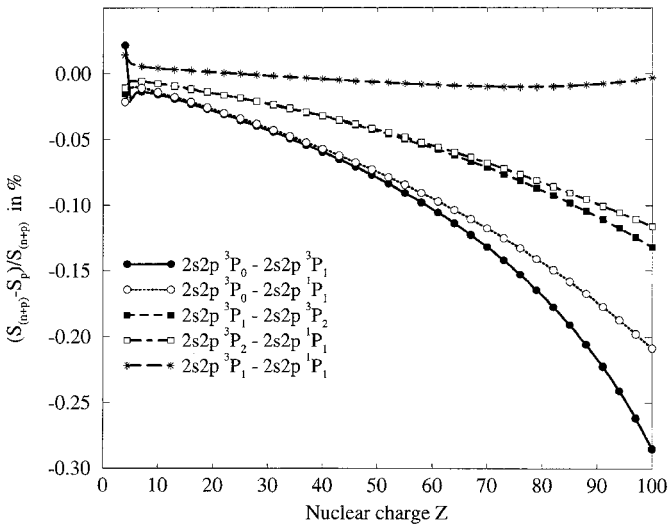

Fig. 3. Z-dependence of the ratio $(S_{n+p} - S_p)/S_{n+p}$ in % for transitions into 2s2p configuration.

3. Results and Discussion

We calculate line strengths and transition probabilities for the 11 M1 transitions inside of $2l2l'$ configurations and the 35 M1 transitions between $2l3l'$ and $2l2l'$ states for all ions up to Z=100. The theoretical energies used to evaluate these transition probabilities are calculated by using second-order MBPT [21].

In Table III, we list the values of line strengths S, calculated for all of the above mentioned M1 transitions. These values are given for $Z = 10$, 20, 40, 60, 80, and 100. We use both LS- and jj-coupling designations to label the levels. We can see from this table, that some LS forbidden transitions with very small S-values for $Z = 10$, 20, for example $2s2p\ ^3P_J$–$2s2p\ ^1P_1$ and 2s2p $^3P_0$ – 2s3p $^1P_1$, become allowed in jj-coupling with substantially larger S-values for high nuclear charges. On the other hand, some LS allowed transitions, for example 2p^2 $^3P_0$ – 2p3p $^3P_1$, become forbidden in the jj-coupling. It should be noted that even though the S-values for transitions inside the same configuration space are much

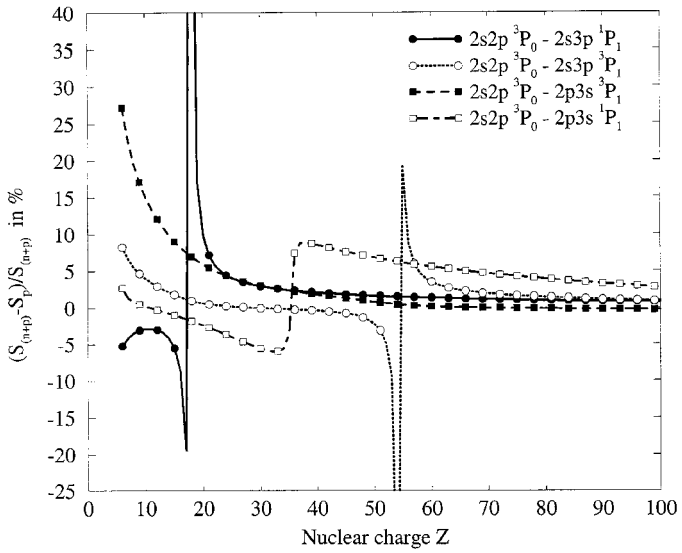

Fig. 4. Z-dependence of the ratio $(S_{n+p} - S_p)/S_{n+p}$ in % for 2–3 transitions.

Table III. *Line strengths* (S) *as function of* Z.

[*LS* designations]		$Z = 10$	$Z = 20$	Z = 40	Z = 60	Z = 80	Z = 100	[*jj* designations]	
$2s2p\ ^3P_0$	$2s2p\ ^3P_1$	2.00(0)	1.99(0)	1.72(0)	1.47(0)	1.39(0)	1.37(0)	2s2p*[0]	2s2p*[1]
$2s2p\ ^3P_0$	$2s2p\ ^1P_1$	6.73(−5)	9.67(−3)	2.77(−1)	5.10(−1)	5.67(−1)	5.50(−1)	2s2p*[0]	2s2p[1]
$2p^2\ ^3P_1$	$2p^2\ ^3P_2$	2.50(0)	2.36(0)	2.12(0)	9.21(−1)	9.03(−1)	9.49(−1)	2s*2p[1]	2s2p*[2]
$2p^2\ ^3P_1$	$2p^2\ ^1D_2$	8.23(−4)	1.36(−1)	1.38(0)	1.55(0)	1.53(0)	1.43(0)	2p*2p[1]	2p2p[2]
$2s^2\ ^1S_0$	$2p^2\ ^3P_1$	2.21(−6)	2.45(−4)	6.36(−3)	1.30(−2)	1.28(−2)	1.08(−2)	2s2s[0]	2p*2p[1]
$2s^2\ ^1S_0$	$2s3s\ ^3S_1$	1.90(−7)	4.46(−6)	8.58(−5)	4.91(−4)	1.77(−3)	5.09(−3)	2s2s[0]	2s3s[1]
$2p^2\ ^3P_0$	$2p3p\ ^3D_1$	2.26(−8)	7.26(−6)	3.07(−4)	1.74(−3)	5.99(−3)	1.59(−2)	2p*2p*[0]	2p*3p[1]
$2p^2\ ^1S_0$	$2p3p\ ^3S_1$	1.15(−7)	2.17(−7)	2.54(−4)	1.89(−3)	7.68(−3)	2.56(−2)	2p2p[0]	2p3p*[1]
$2p^2\ ^1S_0$	$2p3p\ ^3P_1$	5.30(−7)	1.88(−5)	2.17(−4)	9.36(−4)	2.93(−3)	7.24(−3)	2p2p[0]	2p3p[1]
$2s2p\ ^1P_1$	$2s3p\ ^3P_0$	6.01(−7)	1.46(−5)	3.34(−4)	2.01(−3)	7.85(−3)	2.57(−2)	2s2p[1]	2s3p*[0]
$2s2p\ ^3P_0$	$2s3p\ ^3P_1$	1.80(−7)	6.30(−6)	8.89(−5)	5.94(−5)	6.68(−4)	2.19(−3)	2s2p*[0]	2s3p[1]
$2s2p\ ^3P_0$	$2p3s\ ^3P_1$	1.16(−7)	3.14(−6)	1.03(−4)	1.04(−3)	3.17(−3)	8.13(−3)	2s2p*[0]	2p*3s[1]

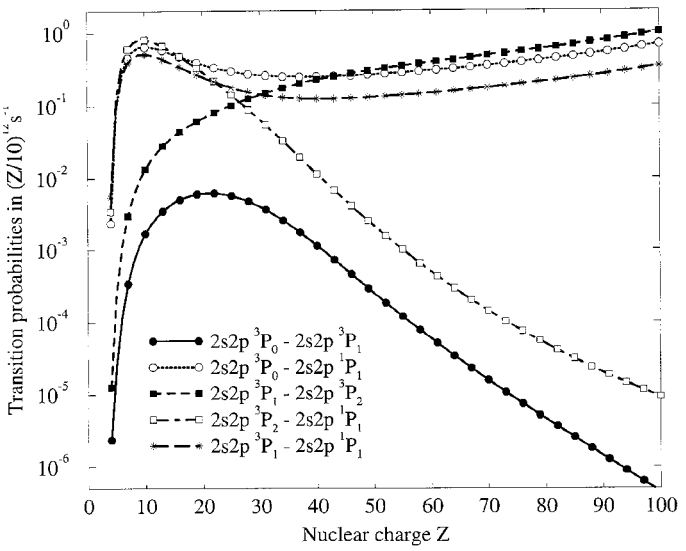

Fig. 5. Z-dependence of transition probabilities A into 2s2p configuration.

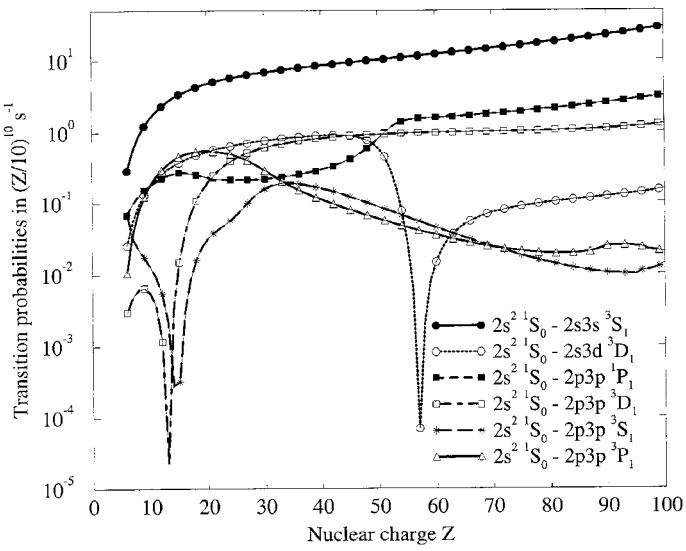

Fig. 6. Z-dependence of transition probabilities A between $2s^2\ ^1S_0$ levels and 6 even parity $2l3l'$ levels with $J = 1$.

larger than the S-values for transitions between different configurations, the A-values for transition probabilities are of the same order. This is explained by small energy differences for transitions inside the same configuration space. The

Table IV. *Transition probabilities* A (s^{-1}) *for* M*1 transition in* $1s^22p^2$ *and* $1s^22s^2$ *configurations as function of* Z: *a – present calculations, b – Glass (1983).*

Z		$^3P_0 - {}^3P_1$	$^3P_1 - {}^3P_2$	$^3P_2 - {}^1P_1$	$^3P_0 - {}^1P_1$	$^3P_1 - {}^1P_1$
6	a	2.68(–7)	2.50(–6)	8.28(–4)	6.12(–4)	5.52(–4)
6	b	2.16(–7)	2.14(–6)	1.98(–3)	1.59(–3)	5.68(–3)
7	a	4.74(–6)	4.11(–5)	8.42(–3)	6.36(–3)	5.42(–3)
7	b	4.28(–6)	3.76(–5)	1.63(–2)	1.32(–2)	3.72(–2)
8	a	4.75(–5)	3.92(–4)	5.14(–2)	3.97(–2)	3.28(–2)
8	b	4.50(–5)	3.71(–4)	8.77(–2)	7.13(–2)	1.63(–1)
9	a	3.25(–4)	2.60(–3)	2.28(–1)	1.79(–1)	1.45(–1)
9	b	3.10(–4)	2.46(–3)	3.41(–1)	2.80(–1)	5.49(–1)
10	a	1.69(–3)	1.33(–2)	8.11(–1)	6.51(–1)	5.17(–1)
10	b	1.63(–3)	1.28(–2)	1.15(+0)	9.57(–1)	1.63(+0)
11	a	7.15(–3)	5.60(–2)	2.45(+0)	2.01(+0)	1.57(+0)
12	a	2.57(–2)	2.02(–1)	6.49(+0)	5.47(+0)	4.22(+0)
12	b	2.52(–2)	1.96(–1)	8.53(+0)	7.40(+0)	2.05(+0)
13	a	8.12(–2)	6.46(–1)	1.56(+1)	1.35(+1)	1.03(+1)
14	a	2.30(–1)	1.87(+0)	3.43(+1)	3.09(+1)	2.32(+1)
14	b	2.27(–1)	1.83(+0)	4.29(+1)	3.95(+1)	1.36(+0)
15	a	5.94(–1)	4.98(+0)	7.04(+1)	6.62(+1)	4.88(+1)
16	a	1.42(+0)	1.24(+1)	1.36(+2)	1.34(+2)	9.74(+1)
17	a	3.16(+0)	2.89(+1)	2.50(+2)	2.60(+2)	1.85(+2)
18	a	6.65(+0)	6.40(+1)	4.38(+2)	4.84(+2)	3.39(+2)
18	b	6.61(+0)	6.33(+1)	5.12(+2)	5.76(+2)	2.33(+2)
19	a	1.32(+1)	1.36(+2)	7.37(+2)	8.71(+2)	5.98(+2)
20	a	2.51(+1)	2.77(+2)	1.19(+3)	1.52(+3)	1.02(+3)
20	b	2.49(+1)	2.73(+2)	1.36(+3)	1.76(+3)	1.02(+3)
21	a	4.55(+1)	5.44(+2)	1.87(+3)	2.59(+3)	1.71(+3)
22	a	7.92(+1)	1.04(+3)	2.84(+3)	4.32(+3)	2.78(+3)
23	a	1.33(+2)	1.91(+3)	4.20(+3)	7.04(+3)	4.44(+3)
24	a	2.15(+2)	3.45(+3)	6.05(+3)	1.13(+4)	6.95(+3)
25	a	3.38(+2)	6.07(+3)	8.50(+3)	1.78(+4)	1.07(+4)
26	a	5.14(+2)	1.04(+4)	1.17(+4)	2.76(+4)	1.63(+4)
26	b	5.06(+2)	1.05(+4)	1.24(+4)	3.03(+4)	1.23(+4)

A-values for the 2–2 transitions are proportional to Z^{12}, since the leading term of S is constant and the energy difference is proportional to Z^4. The magnetic-dipole A-values for the 2–3 transitions are proportional to Z^{10}, since the leading term of S is proportional to Z^4 and the energy difference is proportional to Z^2.

The Z dependence of transition probabilities for the five transitions between levels of 2s2p configurations are shown in Fig. 5. The A-values for six transitions with the initial level $2s^2\ ^1S_0$ and the 6 even parity $2l3l'$ levels with $J = 1$ are shown in Fig. 6. We see from these plots that the A-values for these transitions increase from 10^{-5} s^{-1} to 10^{11} s^{-1} in the interval

Table V. *Transition probabilities* A (s^{-1}) *for* M*1 transition in* $1s^2 2p^2$ *and* $1s^2 2s^2$ *configurations as function of* Z: *a – present calculations, b – Glass (1983).*

Z		$2s^2\ ^1S_0 - 2p^2\ ^3P_1$	$^3P_0 - {}^3P_1$	$^3P_1 - {}^3P_2$	$^3P_1 - {}^1S_0$	$^3P_1 - {}^1D_2$	$^3P_2 - {}^1D_2$
			$2p^2$ LSJ – $2p^2$ L′S′J′				
6	a	6.53(–4)	4.52(–7)	1.73(–6)	4.68(–3)	1.16(–5)	3.64(–5)
6	b	5.33(–4)	4.09(–7)	1.32(–6)	1.92(–2)	1.98(–4)	6.30(–4)
7	a	5.82(–3)	7.29(–6)	2.81(–5)	5.51(–2)	3.33(–4)	1.01(–3)
7	b	4.63(–3)	6.85(–6)	2.44(–5)	1.57(–1)	2.05(–3)	6.59(–3)
8	a	3.30(–2)	6.93(–5)	2.73(–4)	3.69(–1)	3.30(–3)	9.79(–3)
8	b	2.69(–2)	6.61(–5)	2.46(–4)	8.31(–1)	1.25(–2)	3.97(–2)
9	a	1.40(–1)	4.65(–4)	1.83(–3)	1.75(+0)	1.96(–2)	5.65(–2)
9	b	1.17(–1)	4.47(–4)	1.69(–3)	3.36(+0)	5.61(–2)	1.74(–1)
10	a	4.83(–1)	2.44(–3)	9.40(–3)	6.52(+0)	8.55(–2)	2.38(–1)
10	b	4.41(–1)	2.36(–3)	8.38(–3)	1.13(+1)	2.04(–1)	6.09(–1)
11	a	1.43(+0)	1.06(–2)	3.93(–2)	2.05(+1)	3.03(–1)	8.12(–1)
12	a	3.75(+0)	3.97(–2)	1.40(–1)	5.62(+1)	9.27(–1)	2.36(+0)
12	b	5.06(+0)	4.04(–2)	1.37(–1)	7.34(+1)	1.72(+0)	3.99(+0)
13	a	8.94(+0)	1.33(–1)	4.34(–1)	1.39(+2)	2.53(+0)	6.11(+0)
14	a	1.97(+1)	4.08(–1)	1.20(+0)	3.17(+2)	6.34(+0)	1.44(+1)
14	b	2.55(+1)	4.27(–1)	1.20(+0)	3.97(+2)	1.05(+1)	2.19(+1)
15	a	4.09(+1)	1.16(+0)	3.03(+0)	6.72(+2)	1.49(+1)	3.13(+1)
16	a	8.00(+1)	3.09(+0)	7.02(+0)	1.34(+3)	3.29(+1)	6.42(+1)
17	a	1.49(+2)	7.79(+0)	1.50(+1)	2.55(+3)	6.99(+1)	1.25(+2)
18	a	2.68(+2)	1.88(+1)	3.00(+1)	4.65(+3)	1.43(+2)	2.35(+2)
18	b	3.36(+2)	2.09(+1)	3.09(+1)	5.58(+3)	2.09(+2)	3.19(+2)
19	a	4.63(+2)	4.33(+1)	5.60(+1)	8.15(+3)	2.84(+2)	4.27(+2)
20	a	7.77(+2)	9.64(+1)	9.81(+1)	1.38(+4)	5.50(+2)	7.55(+2)
20	b	8.91(+2)	1.10(+2)	1.01(+2)	1.69(+4)	7.72(+2)	1.00(+3)
21	a	1.26(+3)	2.07(+2)	1.62(+2)	2.28(+4)	1.04(+3)	1.31(+3)
22	a	2.01(+3)	4.31(+2)	2.52(+2)	3.65(+4)	1.92(+3)	2.25(+3)
23	a	3.12(+3)	8.69(+2)	3.72(+2)	5.73(+4)	3.46(+3)	3.79(+3)
24	a	4.75(+3)	1.70(+3)	5.21(+2)	8.81(+4)	6.10(+3)	6.34(+3)
25	a	7.09(+3)	3.25(+3)	6.98(+2)	1.33(+5)	1.05(+4)	1.05(+4)
26	a	1.04(+4)	6.03(+3)	8.99(+2)	1.97(+5)	1.77(+4)	1.71(+4)
26	b	1.36(+4)	7.89(+3)	9.58(+2)	2.31(+5)	2.22(+4)	1.95(+4)

of $Z = 6$ – 100. The Z dependence for the A-value of transitions inside the same configuration space, shown in Fig. 5, is rather smooth, compared to that of the 2–3 transitions, presented in Fig. 6. The Z dependence for the 2–3 transitions is more complex reflecting the tangled behavior of the mixing coefficients.

In Tables IV and V, we present wavelengths λ (Å), line strengths S (a.u.), and transition probabilities A (s^{-1}) for five transitions $^3P_0$ – $^3P_1$, $^3P_1$ – $^3P_2$, ^3P_J – $^1P_1$ within the 2s2p configuration, five transitions $^3P_0$ – $^3P_1$, $^3P_1$ – $^3P_2$, $^3P_1$ – $^1S_0$, $^3P_1$ – $^1D_2$, $^3P_2$ – $^1D_2$ within the $2p^2$ configuration, and for the transition between $2s^2\ ^1S_0$ and $2p^2\ ^3P_1$ levels. It is worth noting that the transition $2s^2\ ^1S_0 - 2p^2\ ^3P_1$ is nonrelativistically allowed only due to configuration mixing. (The model space for the $2s^2\ ^1S_0$ level includes three two-particle states: $2s2s[0] + 2p_{1/2}2p_{1/2}[0] + 2p_{3/2}2p_{3/2}[0]$.) In the Tables IV and V, we compare our data for $Z = 6 – 26$ with the other theoretical results [5–7]. All theoretical values agree for LS-allowed transitions: $^3P_0$ – $^3P_1$, $^3P_1$ – $^3P_2$ transitions in 2s2p and $2p^2$ configurations. Such agreement can be expected, since correlation and relativistic effects do not affect these transitions. For these four transitions, the line strengths are almost independent of Z; $S \simeq 2$ for $^3P_0$ – $^3P_1$ transitions and $S \simeq 5/2$ for $^3P_1$ – $^3P_2$ transitions. The corresponding A-value can be accurately determined from the transition energies, which can be obtained from precise spectroscopic data. The experimental A-value of 74(4) s^{-1} for the LS-allowed $2s2p\ ^3P_1$ – $2s2p\ ^3P_2$ transition in Ar^{+14} has been recently reported in Ref. [8]. This value disagrees with previous theoretical results, 63.3 s^{-1} [6] and 63.0 s^{-1} [7]; it also disagrees with our predictions 64.0 s^{-1}, obtained with the MBPT energies and 63.8 s^{-1} obtained with experimental energies.

In contrast to the LS-allowed transitions, we disagree with the previous theoretical values for transitions with $\Delta S = 1$. The A-values for transitions with $\Delta S = 1$ are determined by the mixing coefficients, which are very sensitive to the theoretical approximation employed. Our coefficients were obtained as the result of diagonalizing the first-order effective relativistic Hamiltonian. On the other hand, the LS-coupling scheme was employed in papers [5,6] and the Breit-Pauli approximation was used for relativistic corrections. Owing to the common approach used in [5] and [6], the results of these papers are in a much better agreement with each other than with our results, especially for small Z. Further analysis is necessary to assess the accuracy of two approaches.

4. Conclusion

We have presented a systematic second-order relativistic MBPT study of reduced matrix elements, line strengths, and transition rates for two types of magnetic dipole transitions: with and without change of principle quantum number. The calculations involving a change of principal quantum number are completely new for Be-like ions. In order to confirm the correctness of our method, we also investigated the well-known transitions inside one configuration and we obtained good agreement with other calculations for

LS-allowed transitions where relativistic corrections are not very important. We believe that our results for intercombination transitions are more accurate than previous theoretical results since we treat relativistic contributions more carefully. Contributions from negative-energy states were also included in the second-order matrix elements. It was shown that these contributions are very important for 2–3 transition probabilities. Matrix elements from the present calculations provide basic theoretical input for calculations of reduced matrix elements, oscillator strengths, and transition rates in three-electron boron-like ions.

Acknowledgments

The work of WRJ and AD was supported in part by National Science Foundation Grant No. PHY-95-13179. UIS acknowledges partial support by Grant No. B336454 from Lawrence Livermore National Laboratory.

References

1. Krueger, T. K. and Czyzak, S. A., Astrophys. J. **144**, 1194 (1966).
2. Nusbaumer, H. and Storey, P. J., Astron. Astrophys. **64**, 139 (1978).
3. Nusbaumer, H. and Storey, P. J., J. Phys. B: At. Mol. Phys. **12**, 1647 (1979.
4. Tunnel, T. W. and Bhalla, C. P., Phys. Lett. **72A**, 19 (1979).
5. Oboladze, N. S. and Safronova, U. I., Opt. Spectrosc. **48**, 469 (1980).
6. Glass, R., Astrophys. Space Sci. **91**, 417 (1983).
7. Idress, M. and Das, B. P., J. Phys. B: At. Mol. Phys. **22**, 3609 (1989).
8. Moehs, D. P., and Church, D. A., Phys. Rev. A **58**, 1111 (1998).
9. Kaufman, V. and Sugar, J., J. Phys. Chem. Ref. Data **15**, 321 (1986).
10. Safronova, U. I, Johnson, W. R., Safronova, M. S. and Derevianko, A., Physica Scripta **59**, 286 (1999).
11. Johnson, W. R., Plante, D. R. and Sapirstein, J., Adv. At., Mol. Opt. Phys. **35**, 255 (1995).
12. Feinberg, G. and Sucher, J., Phys. Rev. Lett. **26**, 681 (1971).
13. Drake, G. W. F., Phys. Rev. A **3**, 908 (1971).
14. Beigman, I. L. and Safronova, U. I., Zh. Eksp. Theor. Fiz. **60**, 2045 (1971).
15. Lindroth, E. and Salamonson, S., Phys. Rev. A **41**, 4659 (1990).
16. Indelicato, P., Phys. Rev. Lett. **77**, 3323 (1996).
17. Chen, M. H., Cheng, K. T. and Johnson, W. R., Phys. Rev. A **47**, 3692 (1993).
18. Sucher, J., Phys. Rev. A**22**, 348 (1980).
19. Mittleman, M. H., Phys. Rev. A **4**, 893 (1971); Phys. Rev. A **5**, 2395 (1972); Phys. Rev. A **24**, 1167 (1981).
20. Derevianko, A., Savukov, I., Johnson, W. R and Plante, D. R., Phys. Rev. A (1998).
21. Safronova, M. S., Johnson, W. R. and Safronova, U. I., Phys. Rev. A **53**, 4036 (1996).

